

Quantum interferences in resonant multiphoton-ionization processes for a strongly coupled atomic system

R. S. D. Sihombing, M. Katsuragawa, G. Z. Zhang,* and K. Hakuta

Department of Applied Physics and Chemistry, and Institute for Laser Science, University of Electro-Communications, Chofu, Tokyo 182, Japan

(Received 11 March 1996)

The resonant multiphoton-ionization (MPI) processes in a strongly coupled atomic system have been investigated theoretically and experimentally using atomic hydrogen as a test medium. The characteristics are described with a parameter NL : the product of atom density and interaction length. The MPI characteristics exhibit a single-atom behavior revealing an Autler-Townes doublet in the low- NL region. In the high- NL region, the Autler-Townes doublet is suppressed to almost zero. This phenomenon is shown to be due to destructive interference between the excitation channels to the strongly coupled upper states. It is also shown that a narrow Doppler-free MPI peak appears at the split center of the Autler-Townes doublet in the high- NL region as a consequence of the strong coupling and the propagation effect. [S1050-2947(96)01208-5]

PACS number(s): 42.50.Hz, 42.65 Ky, 32.80.Fb, 42.50.Gy

Many works [1] have been reported regarding interferences in multiphoton-ionization (MPI) processes, including ionization suppression, disappearance of MPI signals with increasing vapor pressure, and reappearance with retroreflection of the pumping laser radiation. However, all these works have been restricted to the interferences under weak-coupling conditions, where bare atomic wave functions can describe the atomic eigenstates well. In the present paper, we extend the quantum interferences in the MPI processes to a strongly coupled atomic system, where atomic eigenstates are described well by dressed atomic wave functions. We investigated these problems theoretically and experimentally using atomic hydrogen as a test medium.

Figures 1(a) and 1(b) illustrate the energy schemes for the present MPI system in terms of two different basis-set expressions: (a) the bare atomic basis expression and (b) the dressed basis expression. In Fig. 1(a), three levels of atomic hydrogen—ground-state $1s$ and two upper states $2s$ and $3p$ —are denoted as $|1\rangle$, $|2\rangle$, and $|3\rangle$, respectively. Laser radiation with a wavelength of 656 nm, ω_c , was applied to the atom to strongly couple the metastable state $|2\rangle$ with state $|3\rangle$, leading to a pair of dressed states $|2d\rangle$ and $|3d\rangle$, which can be expressed as a linear combination of bare atomic basis functions. Laser radiation with a wavelength of 243 nm, ω_e , was used to couple the state $|2\rangle$ with the ground state $|1\rangle$ through a two-photon excitation process. Due to the nonlinear sum-frequency generation (SFG) process, the radiation may be generated at $\omega_g = 2\omega_e + \omega_c$, 103 nm, which couples the upper state $|3\rangle$ with the state $|1\rangle$ through a single-photon excitation process. The MPI processes may occur as photoionization processes from the upper two states with strong laser fields at ω_e and ω_c . Typical photoionization rates are estimated to be 3×10^9 and $3 \times 10^8 \text{ s}^{-1}$ for bare states $|3\rangle$ and

$|2\rangle$ respectively, assuming focused intensities of 40 MW/cm^2 for both strong-coupling and two-photon excitation laser fields [2,3]. The photoionization rate of state $|3\rangle$ far exceeds its spontaneous emission rate Γ_{31} , $1.6 \times 10^8 \text{ s}^{-1}$ [5], and the decay rates of the upper states are mainly governed by the photoionization rates.

The optical responses of the atomic system can be calculated by obtaining the susceptibilities through the equations for time-varying single-atom probability amplitudes. The MPI rate may also be calculated as a loss rate of ground-state atoms. As described in detail in Ref. [4], linear and nonlinear optical susceptibilities $\chi_D^{(L)}$ and $\chi_D^{(NL)}$ and the photoionization rate $\Gamma^{(MPI)}$ are expressed using the dressed-state basis set as

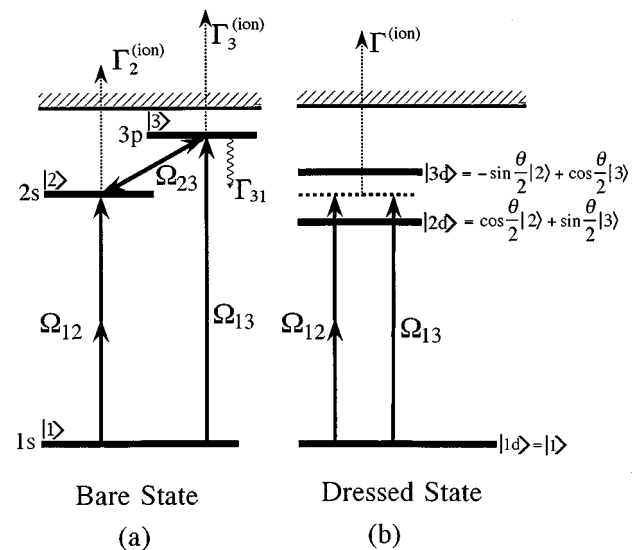


FIG. 1. Energy scheme of atomic hydrogen for resonant multiphoton-ionization processes under strong-coupling conditions by two different basis-set expressions: (a) the bare atomic basis expression and (b) the dressed basis expression.

*Present address: Department of Physics, University of Toronto, Toronto, Ontario, Canada M5S 1A7.

$$\chi_D^{(L)}(-\omega_g, \omega_g) = \frac{N|\mu_{13}|^2}{\varepsilon_0\hbar} \left[\frac{\Delta\omega_{2d}\cos^2\frac{\theta}{2} + \Delta\omega_{3d}\sin^2\frac{\theta}{2} + i\frac{\Gamma_2}{2}}{\Delta\tilde{\omega}_{2d}^*\Delta\tilde{\omega}_{3d}^* + \kappa^2} \right], \quad (1)$$

$$\chi_D^{(NL)}(-\omega_g, \omega_e, \omega_e) = \frac{N\mu_{13}\alpha_{21}}{\varepsilon_0\hbar^2} \left[\frac{(\Delta\omega_{3d} - \Delta\omega_{2d})\sin\theta}{\Delta\tilde{\omega}_{2d}^*\Delta\tilde{\omega}_{3d}^* + \kappa^2} \right], \quad (2)$$

$$\Gamma^{(\text{MPI})} = -\frac{1}{2} \text{Im} \left[\frac{|\Omega_{12}^{(d)}|^2\Delta\tilde{\Omega}_{3d}^* + |\Omega_{13}^{(d)}|^2\Delta\tilde{\Omega}_{2d}^* + 2i\kappa \text{Re}[\Omega_{12}^{(d)}\Omega_{31}^{(d)}]}{\Delta\tilde{\omega}_{2d}^*\Delta\tilde{\omega}_{3d}^* + \kappa^2} \right], \quad (3)$$

where

$$\begin{aligned} \Omega_{12}^{(d)} &= \Omega_{12}\cos\frac{\theta}{2} + \Omega_{13}\sin\frac{\theta}{2}, & \Omega_{13}^{(d)} &= -\Omega_{12}\sin\frac{\theta}{2} + \Omega_{13}\cos\frac{\theta}{2}, \\ \Delta\tilde{\omega}_{2d} &= \Delta\omega_{2d} - \frac{i}{2}\Gamma_{2d} = \omega_2 - \delta - 2\omega_e - \frac{i}{2}\Gamma_{2d}, \\ \Delta\tilde{\omega}_{3d} &= \Delta\omega_{3d} - \frac{i}{2}\Gamma_{3d} = \omega_3 + \delta - \omega_g - \frac{i}{2}\Gamma_{3d}, \\ \kappa &= -\frac{1}{4}(\Gamma_3 - \Gamma_2)\sin\theta, \end{aligned} \quad (4)$$

and

$$\begin{aligned} \Gamma_{2d} &= \Gamma_2\cos^2\frac{\theta}{2} + \Gamma_3\sin^2\frac{\theta}{2}, & \Gamma_{3d} &= \Gamma_2\sin^2\frac{\theta}{2} + \Gamma_3\cos^2\frac{\theta}{2}, \\ \delta &= \frac{1}{2}(\sqrt{\Delta^2 + \Omega_{32}^2} - |\Delta|), & \tan\theta &= \frac{\Omega_{23}}{|\Delta|}, & \Delta &= \omega_3 - \omega_2 - \omega_c. \end{aligned}$$

$\Omega_{12}^{(d)}$ and $\Omega_{13}^{(d)}$ are Rabi frequencies for the $|1d\rangle$ - $|2d\rangle$ and $|1d\rangle$ - $|3d\rangle$ transitions. $\Delta\tilde{\omega}_{2d}$ and $\Delta\tilde{\omega}_{3d}$ represent complex frequency detunings for the dressed states $|2d\rangle$ and $|3d\rangle$. Γ_{2d} and Γ_{3d} are decay rates of the states $|2d\rangle$ and $|3d\rangle$. κ expresses the interference between decay channels for the two dressed states and δ is designated as the effective Rabi splitting of the two dressed states. $\Omega_{13} = \mu_{13}E_g/\hbar$ and $\Omega_{23} = \mu_{23}E_c/\hbar$ are the respective one-photon Rabi frequencies for the generated radiation (ω_g) and the strong-coupling field (ω_c). Ω_{12} is defined as an effective two-photon Rabi frequency for the laser field at ω_e , $\Omega_{12} = \alpha_{12}E_e^2/\hbar$, where $\alpha_{12} = \sum_i \nu_{1i}\mu_{i2}/2\hbar(\omega_i - \omega_e)$, and the terms μ_{ij} stand for the pertinent matrix elements. E_e , E_c , and E_g are the amplitudes of the applied fields. Ω_{23} and Ω_{12} are chosen to have real, positive values. As discussed previously [3,4], the linear and nonlinear susceptibilities reveal destructive and constructive interferences at the split center of the dressed states, respectively. The destructive interference in the linear susceptibility is termed as electromagnetically induced transparency (EIT) [6,7]. The total MPI rate $\Gamma^{(\text{MPI})}$ consists of three terms. The first and second terms represent the MPI processes induced from the two excitation channels $\Omega_{12}^{(d)}$ and $\Omega_{13}^{(d)}$ via the two dressed states $|2d\rangle$ and $|3d\rangle$, respectively. The third term expresses a cross term between the two-excitation channels. Since the dressed Rabi frequencies $\Omega_{12}^{(d)}$ and $\Omega_{13}^{(d)}$ are

defined as linear combinations of Ω_{12} and Ω_{13} , the amplitude and phase relation between Ω_{12} and Ω_{13} may play a critical role in the MPI rate.

The amplitude and phase relation between Ω_{12} and Ω_{13} can be derived theoretically by solving the propagation equation. As described in Ref. [8], the amplitude of the generated radiation including phase can be expressed using the dressed susceptibilities as

$$\begin{aligned} E_g &= \frac{1}{2} \frac{\chi_D^{(NL)}(-\omega_g, \omega_e, \omega_e)}{\chi_D^{(L)}(-\omega_g, \omega_g)} \\ &\times \left\{ \exp \left[i \frac{\omega_g}{2c} \chi_D^{(L)}(-\omega_g, \omega_g)L \right] - 1 \right\} E_e^2, \quad (5) \end{aligned}$$

where L denotes the interaction length between the medium and laser field. Equation (5) illustrates that the amplitude of the generated radiation can be calculated for the propagation in the medium with a parameter NL , the product of the atom density N and the interaction length L .

Next we discuss the MPI characteristics for sufficiently long interaction length, where the exponential term of Eq. (5) tends to zero because of the nonzero residual absorption $\text{Im}[\chi_D^{(L)}]$. The amplitude E_g reaches a stationary value expressed as,

$$E_g = -\frac{1}{2} \frac{\chi_D^{(NL)}(-\omega_g, \omega_e, \omega_e)}{\chi_D^{(L)}(-\omega_g, \omega_g)} E_e^2. \quad (6)$$

Substituting Eqs. (1) and (2) for Eq. (6), one can obtain the relationship between the Rabi frequencies Ω_{13} and Ω_{12} as

$$\Omega_{13} = \frac{1}{2} \frac{(\Delta\omega_{2d} - \Delta\omega_{3d}) \sin\theta}{\Delta\omega_{2d} \cos^2 \frac{\theta}{2} + \Delta\omega_{3d} \sin^2 \frac{\theta}{2} + i \frac{\Gamma_2}{2}} \Omega_{12}. \quad (7)$$

Here we examine the relationships at the dressed states and at the split center of the dressed states. At the dressed states $2d$ and $3d$, the respective Ω_{13} expressions are obtained as

$$\Omega_{13} = -\Omega_{12} \cot \frac{\theta}{2}, \quad \Omega_{12} \tan \frac{\theta}{2}, \quad (8)$$

where we neglect the Γ_2 term, which is much smaller than the detuning $\Delta\omega_{3d}$ ($\Delta\omega_{2d}$) term. It is readily seen from the definition of the dressed Rabi frequencies $\Omega_{12}^{(d)}$ and $\Omega_{13}^{(d)}$ in Eq. (4) that the above Ω_{13} expressions result in zero values of the Rabi frequencies of $\Omega_{12}^{(d)}$ and $\Omega_{13}^{(d)}$ at the resonance positions for the $2d-1d$ and $3d-1d$ transitions, respectively. From this we may conclude that, with an increase of NL , the amplitude of the generated radiation rises to a value at which the single-photon channel exactly cancels the two-photon channel in terms of excitation to the $2d$ and $3d$ states. According to this destructive interference, the MPI rate to the two dressed states may be suppressed to zero in the high- NL region.

At the split center of the two dressed states, where $\Delta\omega_{2d} \cos^2(\theta/2) + \Delta\omega_{3d} \sin^2(\theta/2) = 0$ is satisfied, the Ω_{13} value can increase to a much larger value than the Ω_{12} value. The stationary Ω_{13} value is readily obtained from Eq. (7) as

$$\Omega_{13} = i \frac{\Omega_{23}}{\Gamma_2} \Omega_{12} \quad (9)$$

and the MPI rate at the split center is expressed as

$$\Gamma^{(\text{MPI})} = \frac{|\Omega_{12}|^2 \Gamma_3 + |\Omega_{13}|^2 \Gamma_2}{2|\Omega_{23}|^2}. \quad (10)$$

When the $|\Omega_{13}|$ value far exceeds the $|\Omega_{12}|$ value, the MPI rate at the center may be dominated by the second term, which is proportional to $|\Omega_{13}|^2$. Under high- NL conditions, the MPI characteristics at the split center are governed by the SFG characteristics, including propagation effect, and the spectral profile may be described by Eq. (7). As seen from Eq. (7), the spectral profile gives rise to a sharp peak at the center due to the EIT effect. The final limitation of its width is governed by the decay rate for the two-photon-allowed state $|2\rangle$, not for the state $|3\rangle$, because the resonance at the center is inherently a two-photon resonance.

So far we have not explicitly involved the inhomogeneous Doppler broadening that inevitably accompanies the real gas-phase transitions. However, the formalism developed so far can be applied to the Doppler-broadened systems without any change by assuming the coupling Rabi frequency that far exceeds the Doppler width [7], because such Rabi frequencies can realize strong-coupling conditions for all atoms that

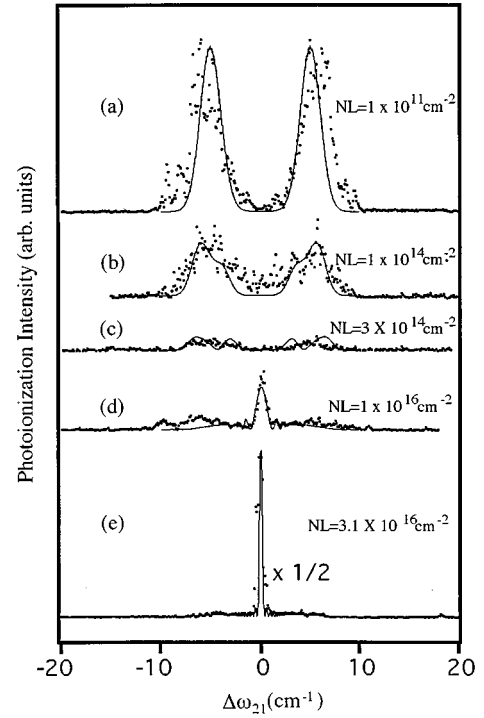


FIG. 2. Tuning characteristic for MPI spectra versus the frequency detuning $\Delta\omega_{21} = \omega_2 - 2\omega_e$ for five different NL values. Solid lines denote the calculated characteristics and black dots correspond to the experimental results. The coupling Rabi frequency Ω_{23} was fixed to 10 cm^{-1} for both the calculations and the experiments. An effective Doppler width of 2.6 cm^{-1} was involved in the calculation for the $3p-1s$ transition at 103 nm .

have various Doppler shifts in the radiation fields. In treating the optical responses systematically for the Doppler-broadened system, the susceptibilities must be numerically calculated by convolving the Gaussian density of states due to the inhomogeneous Doppler broadening.

Figures 2(a)–2(e) display the numerically calculated MPI characteristics versus detuning $\Delta\omega_{21}$ for several of the NL values. The results are drawn as solid lines. The experimental results are marked by black circles. These results are discussed later. The coupling laser was assumed to be set on resonance to the $3p-2s$ transition. An effective Doppler broadening was estimated to be 2.6 cm^{-1} full width at half maximum (FWHM) [9] and was involved in the calculations for the generated radiation at 103 nm . The coupling and two-photon excitation Rabi frequencies Ω_{23} and Ω_{12} were assumed to be 10 and 0.001 cm^{-1} , respectively. Here the coupling Rabi frequency far exceeds the Doppler width and the strong-coupling condition is well satisfied. As seen from the figures, the calculations predict that, in the low- NL region, the characteristics are well described by the single-atom characteristics: the two peaks appear at the dressed states, revealing the Autler-Townes doublet, and their profiles correspond to the Doppler profiles. With the increase of the NL value the doublet peaks are suppressed and at the NL value of $3.1 \times 10^{16} \text{ cm}^{-2}$ the doublet peaks almost disappear. This behavior clearly reveals that with an increase of NL , Ω_{13} increases to $\mp\Omega_{12}$ at the doublet-peak positions for $2d$ and $3d$, respectively, and that the excitation channels to the $2d$ and $3d$ states are canceled due to the destructive interfer-

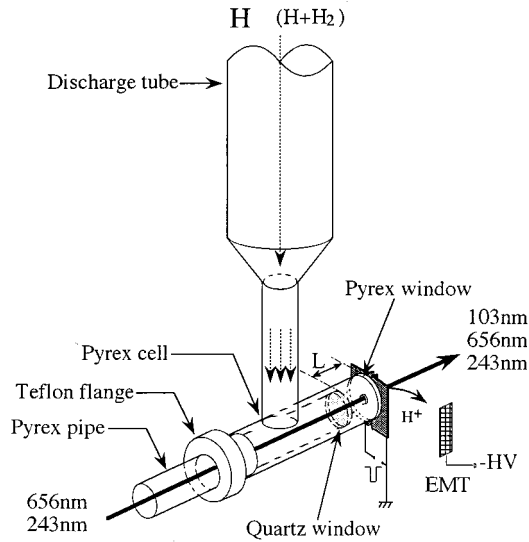


FIG. 3. Schematic diagram of an atomic-hydrogen cell system.

ences. At the split center, a single peak appears in the high- NL region and with the increase of NL the peak rises to produce a much narrower spectral width than the Doppler width. The width is about 0.36 cm^{-1} FWHM at $NL=3.1 \times 10^{16} \text{ cm}^{-2}$. This narrow width is an important consequence of the strong coupling. Since the Doppler tail decreases much more quickly with the detuning than the Lorentzian tail, the $|\chi_D^{(L)}|$ behavior at the split center can basically be described by the behaviors of Lorentzian and dispersion tails under the strong-coupling condition. Thus the MPI profile at the center results in a narrow Doppler-free profile, essentially expressed by Eq. (7). As expected from the theoretical considerations above, this sharp Doppler-free profile corresponds to a profile for SFG characteristics in the high- NL region presented in Fig. 6 of Ref. [4]. We assumed a resonant-coupling condition for the $3p$ - $2s$ transition in our numerical calculations, but obviously the resonant coupling is not an essential issue for observing these characteristics. The same characteristics can be obtained for the detuned-coupling case, if the laser intensity is strong enough to satisfy the condition of $\theta \approx \pi/2$.

Experiments were carried out using an atomic hydrogen apparatus and two single-longitudinal-mode pulsed dye lasers at 656 and 243 nm [10]. Here the experimental setup is described briefly. More details have been given in Ref. [4]. The 656-nm laser beam with a pulse duration of 4 ns was used for the coupling of states $3p$ and $2s$ and the 243-nm laser beam with a pulse duration of 3 ns for two-photon excitation between the $2s$ and $1s$ states. The 656-nm laser was set on resonance to the $3p$ - $2s$ transition. The MPI characteristics were measured by scanning the 243-nm laser for the $2s$ - $1s$ two-photon transition. Both laser beams for coupling and two-photon excitation were loosely focused to the interaction region, leading to parallel beams with diameters of 0.7 and 0.5 mm, respectively. Focused intensities of both lasers were kept at 40 MW/cm^2 , which corresponds to the Rabi frequencies Ω_{23} and Ω_{12} of 10 and 0.001 cm^{-1} , respectively. Hydrogen atoms were generated in a microwave discharge of H_2 gas at a pressure between 0.1 and 1 Torr. An atomic beam system was used for low-atom-density experi-

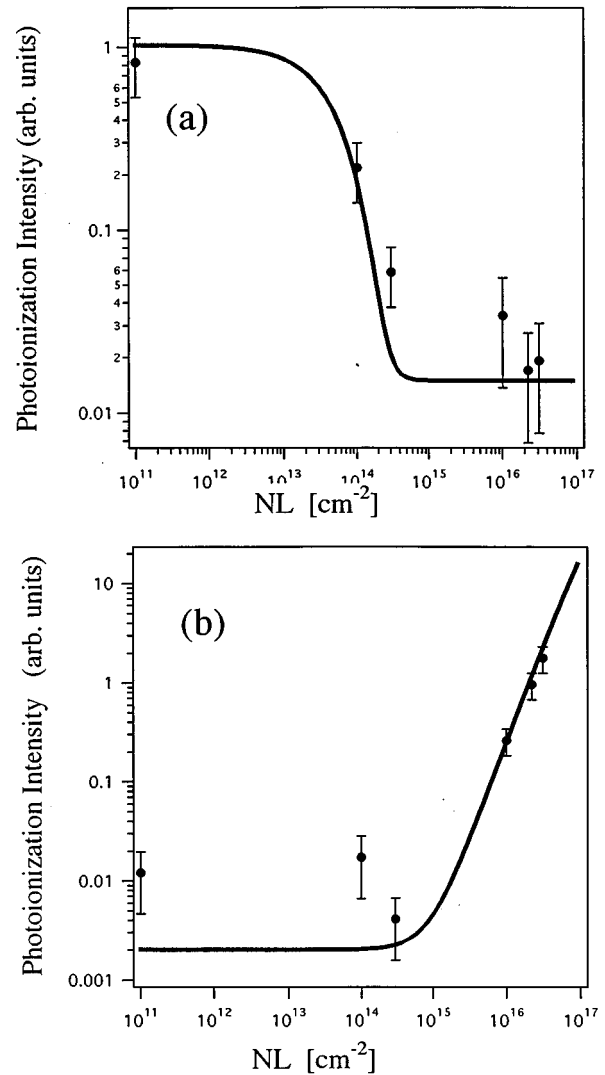


FIG. 4. MPI signal intensities versus the density-length product NL (a) at the Autler-Townes peaks and (b) at the split center. Solid lines denote the calculated characteristics and black circles correspond to the experimental results.

ments and a cell system for high-density experiments. In the atomic beam, the atom density was estimated using the method described in Ref. [11]. The interaction length was varied by changing the number of nozzles. The cell system is schematically displayed in Fig. 3. The H-atom density was estimated to be $1 \times 10^{15} \text{ cm}^{-3}$ in the cell. The incident laser beams enter the interaction region through a quartz window attached to the end of the Pyrex pipe. This pipe can be moved along the direction of laser-beam propagation, which enables variation in the NL value for fixed-atom-density conditions. On the other end of the Pyrex cell, a Pyrex window is attached, at the center of which a hole with a diameter of 0.7 mm has been drilled. Two parallel aluminum plates of 0.7-mm spacing were placed on the outside face of the Pyrex window. Photoions generated between the aluminum plates were detected by applying a pulsed electric field between the plates with a suitable delay time after the incident laser beam.

The observed tuning characteristics are displayed as black

circles in Figs. 2(a)–2(e), which satisfactorily reproduce the predicted characteristics shown by the solid lines. Autler-Townes doublet peaks are clearly observed with Doppler profile at the resonance positions for the dressed states in the low- NL region and the doublet peaks are suppressed to zero with the increase of the NL value. The narrow Doppler-free peak is observed at the split center of the Autler-Townes doublet in the high- NL region. Figures 4(a) and 4(b) show the intensities of photoionization signals versus NL at one peak of the Autler-Townes doublet and at the split center, respectively. Solid lines denote the calculated results. The coupling Rabi frequency Ω_{23} is fixed at 10 cm^{-1} . Both of the results in Figs. 4(a) and 4(b) are normalized to the peak values of the photoionization signal at $NL=1\times 10^{11}\text{ cm}^{-2}$. The MPI signal at the dressed-state position is suppressed by a factor of 40 by increasing NL to $3.1\times 10^{16}\text{ cm}^{-2}$, revealing a good correspondence to the theoretical value of factor 50. The MPI signal at the center appears around $NL=1\times 10^{15}\text{ cm}^{-2}$ and increases quadratically as NL increases. This behavior is understood from the fact that for the low- NL region the MPI signal arises from the two-photon excitation channel through the 243-nm laser radiation, but for the high- NL region it arises from the single-photon excitation channel through the generated radiation at 103 nm whose amplitude rises quadratically with the increase of NL at the split center [4].

In conclusion, we have investigated theoretically and experimentally the resonant MPI processes for a strongly coupled atomic system using atomic hydrogen as a test medium. It has been shown that the MPI characteristics exhibit single-atom behavior revealing the Autler-Townes doublet in the low- NL region, but the Autler-Townes doublet may be suppressed to zero in the high- NL region due to destructive interferences between the excitation channels to the upper dressed states. It has also been shown that a narrow Doppler-free MPI peak appears at the split center of the Autler-Townes doublet in the high- NL region as a consequence of the strong coupling and propagation effect. The narrow spectral profile we have demonstrated may offer an alternative technique in laser spectroscopy for observing two-photon resonances with Doppler-free resolution.

This work was supported by a Grant-in-Aid for Scientific Research in a Priority Area “Mutual quantum manipulation of radiation field and matter” from the Ministry of Education, Science, Sports, and Culture of Japan. The authors acknowledge Dr. F. Currell and A. Currell for a critical reading of the manuscript. One of the authors (R.S.D.S.) deeply thanks the Rotary Yoneyama Foundation for financial support during the course of this study.

-
- [1] J. C. Miller, R. N. Compton, M. G. Payne, and W. R. Garrett, *Phys. Rev. Lett.* **45**, 114 (1980); M. G. Payne and W. R. Garrett, *Phys. Rev. A* **26**, 356 (1982); J. J. Wynne, *Phys. Rev. Lett.* **52**, 751 (1984); W. R. Garrett, S. D. Henderson, and M. G. Payne, *Phys. Rev. A* **34**, 3463 (1986); P. R. Blazewicz and J. C. Miller, *ibid.* **38**, 2863 (1988); M. G. Payne, J. Y. Zhang, and W. R. Garrett, *ibid.* **48**, 2334 (1993).
 - [2] A. Burgess, *Mem. R. Astron. Soc.* **69**, 1 (1965).
 - [3] G. Z. Zhang, K. Hakuta, and B. P. Stoicheff, *Phys. Rev. Lett.* **71**, 3099 (1993).
 - [4] G. Z. Zhang, M. Katsuragawa, K. Hakuta, R. I. Thompson, and B. P. Stoicheff, *Phys. Rev. A* **52**, 1584 (1995).
 - [5] E. U. Condon and G. H. Shortley, *Theory of Atomic Spectra* (Cambridge University Press, Cambridge, 1987), p. 136.
 - [6] A. Imamoglu and S. E. Harris, *Opt. Lett.* **14**, 1344 (1989).
 - [7] S. E. Harris, J. E. Field, and A. Imamoglu, *Phys. Rev. Lett.* **64**, 1107 (1990).
 - [8] K. Hakuta, L. Marmet, and B. P. Stoicheff, *Phys. Rev. A* **45**, 5152 (1992).
 - [9] The effective Doppler broadening represents an inhomogeneous broadening including effects of thermal Doppler broadening and inhomogeneity of the strong-coupling field in both spatial and temporal aspects.
 - [10] M. G. Littman, *Appl. Opt.* **23**, 4465 (1984); G. Z. Zhang and K. Hakuta, *Opt. Lett.* **17**, 997 (1992).
 - [11] L. Marmet, K. Hakuta, and B. P. Stoicheff, *J. Opt. Soc. Am. B*, **9**, 1038 (1992).